ARMY RESEARCH LABORATORY

# Local Fractal Dimension Estimation

by Mark C. Wellman

ARL-TR-517

February 1995

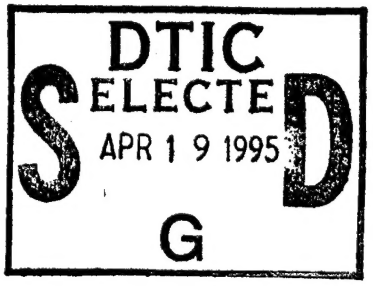

The findings in this report are not to be construed as an official Department of the Army position unless so designated by other authorized documents.

Citation of manufacturer's or trade names does not constitute an official endorsement or approval of the use thereof.

Destroy this report when it is no longer needed. Do not return it to the originator.

# REPORT DOCUMENTATION PAGE

*Form Approved*
*OMB No. 0704-0188*



| 1. AGENCY USE ONLY *(Leave blank)* | 2. REPORT DATE | 3. REPORT TYPE AND DATES COVERED |
|---|---|---|
| | February 1995 | Final, from FY93 to FY94 |

**4. TITLE AND SUBTITLE**
Local Fractal Dimension Estimation

**5. FUNDING NUMBERS**
DA PR: AH44
PE: 611102H44

**6. AUTHOR(S)**
Mark C. Wellman

**7. PERFORMING ORGANIZATION NAME(S) AND ADDRESS(ES)**
U.S. Army Research Laboratory
Attn: AMSRL-SS-SA
2800 Powder Mill Road
Adelphi, MD 20783-1197

**8. PERFORMING ORGANIZATION REPORT NUMBER**
ARL-TR-517

**9. SPONSORING/MONITORING AGENCY NAME(S) AND ADDRESS(ES)**
U.S. Army Research Laboratory
2800 Powder Mill Road
Adelphi, MD 20783-1197

**10. SPONSORING/MONITORING AGENCY REPORT NUMBER**

**11. SUPPLEMENTARY NOTES**
AMS code: 611102.H44
ARL PR: 3AE111

**12a. DISTRIBUTION/AVAILABILITY STATEMENT**
Approved for public release; distribution unlimited.

**12b. DISTRIBUTION CODE**

**13. ABSTRACT** *(Maximum 200 words)*

This study focused on developing a fractal dimension estimator which will be accurate over the limited range of fractal dimensions characteristic of the earth's natural relief. The estimator presented will have the advantage of reduced complexity and processing over the more optimal techniques. Local window estimates will be investigated as well as synthetic fractal surfaces produced from two different synthesis techniques.



**14. SUBJECT TERMS**
Fractals, estimation.

**15. NUMBER OF PAGES**
23

**16. PRICE CODE**

| 17. SECURITY CLASSIFICATION OF REPORT | 18. SECURITY CLASSIFICATION OF THIS PAGE | 19. SECURITY CLASSIFICATION OF ABSTRACT | 20. LIMITATION OF ABSTRACT |
|---|---|---|---|
| Unclassified | Unclassified | Unclassified | UL |

NSN 7540-01-280-5500

Standard Form 298 (Rev. 2-89)
Prescribed by ANSI Std. Z39-18
298-102

# Contents



# Figures



# Tables

# 1. Introduction

Since the work in the late 60's by B. B. Mandelbrot and J. W. Wallis [1], a novel class of mathematical functions known as "fractals" has enjoyed great popularity [2–5]. Fractals are found extensively in nature, and fractal surfaces are produced by a number of basic physical processes like erosion, aggregation, and turbulent flow. These processes modify shape through local iterative actions and thus produce fractals as an end result [4,6,7]. Fractal models are currently in use in a number of areas of image analysis, such as shape from texture [7–9], texture analysis and segmentation [10,11], interpolation of terrain data [12], automatic target recognition [13,14], and medical image analysis [15,26] to name a few. The realism of computer-generated images using fractal models strongly suggests that the model captures relevant perceptual information of the image that appeals to our visual processing system.

## 1.1 Fractal Model and Dimension

A fractal can be loosely defined as a set whose only consistent description of its metric properties requires a noninteger dimension greater than or equal to the standard intuitive definition of a set's dimension. This leads to the notion of the "fractal dimension," which is the consistent measure of the set's roughness and irregularities [7], and has been shown to be twice as accurate as any previous reported measure for perceptual roughness [17]. Fractals are classified into two types: deterministic and random, and whereas deterministic fractals show self-similarity over all scales, random fractals are self-affine over a limited range of scales [5]. A sampling of the images one can generate with either type can be found in the references [2–5]. Random fractals, which are of most interest to the scientific community, will be the primary concern of this report.

A useful mathematical model for random fractals, as proposed by Mandelbrot and Van Ness, is fractional Brownian motion (*fBm*) [1], which is a generalization of the familiar Brownian motion. The model is an extension of classical Brownian motion and encompasses a larger group of phenomena.

Let $V(x)$ be a self-affine *fBm* with a Euclidean dimension ($E$) of one, with the increments having zero-mean Gaussian distribution. The variance has the following form:

$$\left\langle |V(x+dx)-V(x)|^2 \right\rangle \propto |dx|^{2H} , \tag{1}$$

and has a fractal dimension $Df$ given by $Df = E + 1 - H$, where the brackets "$\langle$" and "$\rangle$" denote the ensemble averaged over many samples of $V(x)$. $H$

is often called the "persistence" parameter, since it is proportional to the degree of correlation and is bounded above by one and below by zero. The increments are stationary and isotropic, depending only on the difference in $x$, and for $H = 0.5$ we have classical Brownian motion.

$$\left\langle |V(x + dx) - V(x)|^2 \right\rangle \propto |dx| \ . \tag{2}$$

$V(x)$ shows a statistical scaling behavior; i.e., if $x$ is changed by the factor $k$, then the increments of $V(x)$ change by the factor $k$ raised to the $H$.

$$\left\langle dV(kx)^2 \right\rangle \propto \left\langle dV(x)^2 \right\rangle k^{2H} \ . \tag{3}$$

This nonuniform scaling is different in the two coordinates $x$ and $V(x)$ and gives the *fBm* its self-affine property, unlike the self-similar property of deterministic fractals [27]. This will prove important in the selection of a viable fractal dimension estimator [5].

The extension to higher dimensions leads to a fractal Brownian surface (*fBs*), which holds our current interest since it is an excellent model of the earth's terrain [7,12]. Let $V(x,y)$ be a self-affine *fBs* with a Euclidean dimension ($E$) of two with the increments having zero-mean Gaussian distribution. The variance again has the following form:

$$\left\langle |V(x + dx, y + dy) - V(x,y)|^2 \right\rangle \propto \left| dx^2 + dy^2 \right|^H \ , \tag{4}$$

and has a fractal dimension $Df$ given by $Df = E + 1 - H$.

The characterization of a generalized power spectrum for this random process is an extension of the concept of spectral density and the Weiner-Khintchine relation to nonstationary noise [18–20] and takes the form of a random-phase Fourier transform, with the expected value of the power obeying the relationship

$$S(f) \propto f^{-B} \ . \tag{5}$$

Due to the nonstationarity of fractal Brownian processes, a power spectrum cannot be formally defined; however, the increments (derivative) of the random process are stationary, and therefore a power spectrum of the increments can be well-defined. Using this property, Flandrin [21], Keshner [22], and Wornell [23] substantiated the above form of the power spectrum. The decay parameter $B$ is related to the fractal dimension and to the persistence parameter $H$ by

$$B = 2H + E \text{ and } Df = E + 1 - H \ ,$$

where $E$ is the Euclidean dimension and $Df$ the fractal dimension. If any straight-line cut is taken in the $x$ or $y$ direction of a fractal Brownian surface, the spectral density will have the power law in equation (5); this implies that a two-dimensional (2-D) spectral density should behave as

$$S(f) \propto \frac{1}{f^{2H+2}} = f^{-B} \; ; \tag{6}$$

for spatial frequencies $k$ and $l$, $f = \left(k^2 + l^2\right)^{1/2}$ .

A great deal of work has been done in both synthesis and analysis of fractals using this power spectrum relationship [9,13,28,29].

## 1.2 Synthetic Fractal Surfaces

To quote H. E. Schepers et al [24] "production of a truly fractal signal is itself a nontrivial exercise." This truth became very apparent in this study as I found that the only reliable measure of a fractal was careful development of the spectral components, comparison to other authors' images and surfaces, and a portion of faith. The two algorithms used for generating fractal surfaces were the mid-point displacement (MPD) and power spectrum density (PSD) methods. Both are currently popular in the computer graphics community for synthetic scene generation [5,16,27]. The MPD method is a recursive technique first applied by Weiner in the 1920's in modeling Brownian motion. This is a "quick and dirty" algorithm for modeling fractals—quick because of the reduced complexity and execution speed and dirty since it sacrifices mathematical accuracy (and whose result can be seen as visible artifacts on a surface when properly shaded). One should see Pietgen and Saupe [5] for the mechanics of this algorithm as well as some interesting renderings. The PSD method is elaborated on by Voss and others [5,27]. Basically, one creates a discrete Fourier transform (DFT) of the real image $u(m,n)$ for a surface with the 2-D DFT pair given as

$$v(k,l) = \sum_{m=0}^{N-1} \sum_{n=0}^{N-1} u(m,n) W_N^{km} W_N^{ln} \quad 0 \le k, l \le N-1 \tag{7}$$

$$u(m,n) = \frac{1}{N^2} \sum_{k=0}^{N-1} \sum_{l=0}^{N-1} v(k,l) W_N^{-km} W_N^{-ln} \quad 0 \le m, n \le N-1 \; , \tag{8}$$

$$W_N = \exp\left(\frac{-2j\pi}{N}\right) \; , \tag{9}$$

with the phase information derived from a random uniform distribution on $2\pi$. When the DFT coefficients are restricted to have the form

$$\left\langle |v(k,l)|^2 \right\rangle \propto \frac{1}{\left(k^2+l^2\right)^{H+1}} \ , \tag{10}$$

a single realization of the fractal surface will be generated. Alternatively, the form

$$|v(k,l)|^2 \propto \frac{1}{\left(k^2+l^2\right)^{H+1}} \ , \tag{11}$$

will generate the ensemble average. Here $H = 3 - Df$ and $\langle\,\rangle$ denote expected values. For a real image of a fractal surface we must also observe the complex conjugate symmetry,

$$v(k,l) = v^*(N-k, N-l) \quad 0 \le k, l \le N-1 \ ; \tag{12}$$

therefore, our phase requirement—although derived from a random uniform distribution over $2\pi$—has to be zero at the following points: (0,0), (0,$N$/2), ($N$/2,$N$/2), and ($N$/2,0) [5,30].

One can readily observe that this model imposes a bandlimited spectrum, which introduces problems in producing real fractals and especially those with higher fractal dimension values. A second problem is the periodic nature of the surface image created by the inverse fast Fourier transform (FFT). This periodicity "perceptually accentuates the presence of the first spatial-frequency harmonic" [29] of the DFT. The $N/2 \times N/2$ regions of the surface were used for the analysis, as suggested by Voss [31], hopefully to correct this problem.

The MPD surfaces will serve as a useful comparison to the more reliable PSD surfaces in both the fractal dimension calculations and three-dimensional (3-D) renderings of the surface images and DFTs. Also, one must question what effect the artifacts of the MPD method have in determining the fractal dimension of the surfaces created. I was very interested in the results of the estimator with respect to the single-realization PSD surfaces since these surfaces are more representative of natural relief than the ensembles and, therefore, validate the estimator's performance.

## 1.3 Fractal Dimension Estimation

Several techniques have been developed to estimate the fractal dimension as researchers probe for optimality with respect to a particular fractal set [22,23,25]. All the techniques attempt to measure a scaling parameter associated with either a self-similar, statistically self-similar, or self-affine fractal (see Pietgen and Saupe [5] for more). The simplest technique, and quite general in nature, is the Mass Scaling (MS) technique, which makes

no assumptions about the underlying process that created the fractal. In the application to fractal surfaces, the MS technique measures the mass about some central point, i.e., pixel $(x,y,z)$, by counting the number of pixels $M(l)$ that fall within cubes of varying side $l$. The power law requirement for mass distribution is given by

$$M(l) = kl^{Df} \quad , \tag{13}$$

where $Df$ is the fractal dimension and is found by a least-squares fit on the plot of log $(M)$ versus log $(l)$ [5,29,31] and $k$ is the proportionality constant.

Despite improvements to the earlier work of Keller et al [11], the MS technique has some shortcomings; first, the self-affine property creates problems in determining the fractal dimension since scaling may be different in each dimension of a multidimension space as elaborated on by Voss and others [5,31]. Although this problem is cleverly addressed by Moghaddam [29], it is still not completely resolved. Secondly, the MS method is not reliable in the important region-spanning fractal dimension 2.0 to 2.2, which is the predominant range for fractal dimensions of the earth's natural relief [5,9] and is completely unreliable at very high fractal dimensions associated with tree clutter [13,29].

The power spectrum method (PE) is based on the spectral model of fractal Brownian motion, which is more complex and time consuming, but has given excellent results in texture segmentation [7,28] and yields the least biased results and lowest variance in estimates of the fractal dimension regardless of the underlying model used to create the fractal set [24].

The PE estimator in this report will determine the spectral decay parameter $B$ by logarithmic least-squares fit for log (power) versus log (radial frequency) by first taking a local $8 \times 8$ window, zero padding to $16 \times 16$, and computing the FFT. The DFT coefficients are used to calculate the total power of a single or multiple occurrence of a specific radial frequency, and then a logarithmic plot and least-squares fit are applied. The slope $(B)$ is then determined and used to calculate the fractal dimension, which is mapped back to the central four pixels of the $8 \times 8$ window. Finally, the window is slid by two pixels and the process repeated.

The type of windowing function applied to a local sample of the test surface is an area of debate among researchers. The Gabor window applied to the PE method has proven to be very accurate on test images [9]; however, this windowing involves the extra step of convolution that magnifies execution time, albeit with the gain of improved spatial-frequency resolution over the domain of fractal surfaces—i.e., surfaces with fractal dimensions between 2.0 and 3.0. In this study, I am not concerned with performance in the higher fractal dimension regions and, in reality, optimality is not measured solely by the accuracy of the algorithms over the entire range, but by the practicality of implementation, speed, and confidence in estimation accu-

racy over limited ranges. Although a rectangular window has shortcomings due to higher sidelobe energy, the implementation is simple and favors higher frequency resolution. The size of the window was chosen as a compromise between spatial resolution improvement over larger windows and the decreased likelihood of including nonstationary regions when tested against real surfaces. Also, $8 \times 8$ windows seem to be the breakpoint in the variance of the estimate, with windows smaller than $8 \times 8$ being unreliable because of the large variance of the estimated fractal dimension.

The zero padding effectively gives more samples of the 2-D DFT envelope, which is useful in the least-squares fit and is amenable to the FFT calculation. For the decay parameter $B$ calculation, Pentland [7] performed a least-squares fit in the $k$ and $l$ directions of the discrete spatial-frequency plane only, then calculated the $B_x$ and $B_y$ parameters, followed by averaging these $B$ values to determine the fractal dimension. He relied on the fact that most natural fractals exhibit only slight anisotropy [7,16]. Moghaddam [29] improved on the technique by using a weighted least-squares fit based on the number of occurrences of a particular radial frequency in the discrete spatial-frequency plane. The estimator used in this study only modified terms due to a single occurrence of a radial frequency (spatial frequencies where $k = l$), giving these terms equal weight, and although counter-intuitive, gave equivalent results as a simple deweighting algorithm that removed single occurrences of a radial frequency in the DFT before the least-squares fit. The mapping to the central four pixels is based on the observations of Yokoya et al [12]. Their results showed that although the intensity of the fractal surface image does not vary smoothly, the fractal dimension varies smoothly for a real terrain surface. Therefore, a mapping to the central four pixels should not decrease the reliablility of the estimate significantly, but will decrease the number of FFTs performed and least-squares calculations.

# 2. Procedure

A total of three sets of fractal surfaces were synthesized using (1) the MPD method, (2) the PSD method with the DFT magnitudes derived according to the ensemble average expression (eq (11)), and, finally, (3) the PSD method with the DFT magnitudes derived according to the single-realization expression (eq (10)). The fractal dimensions chosen for the global constructs were 2.0, 2.2, 2.4, 2.6, 2.8, and 3.0. The same seed for the random number generator was used for creating all synthetic surfaces. Global constructs were created which were $512 \times 512$, then segmented into four blocks of $256 \times 256$ each. This led to a total of 72 surfaces for estimation purposes.

Estimation of the fractal dimension was performed by first taking a local $8 \times 8$ window, zero padding to $16 \times 16$, and computing the FFT. The spectral decay parameter $B$ was determined as the slope of the logarithmic least-

squares fit for log (power) versus log (radial frequency) and then used to calculate the fractal dimension, which is mapped back to the central four pixels of the $8 \times 8$ window. Finally, the window is slid by two pixels and the process repeated. This generates a $250 \times 250$ array of fractal dimension values for each $256 \times 256$ fractal surface. First- and second-order statistics were calculated for each fractal dimension array.

# 3. Results

A total of 72 surfaces were synthesized and subjected to the PE estimation algorithm. Tables 1 to 3 list the three classes of fractal surfaces created and their estimated fractal dimensions, variance of the estimate, and the contribution to the modified average mean square error (mamse) for each $256 \times 256$ block. The mamse was calculated from a fractal dimension array according to the following [30]:

$$\text{mamse} = \frac{1}{N} \sum_{n=1}^{N} |Df - \overline{Df_n}|^2 , \tag{14}$$

with $Df$ = global fractal dimension for $512 \times 512$ block and $\overline{Df_n}$ = the mean fractal dimension for $n^{\text{th}}$ $256 \times 256$ subblock.

**Table 1. Mean, variance, and mamse of $250 \times 250$ fractal dimension arrays resulting from PE estimation on MPD constructs.**

| File | Fractal dimension estimate | Variance | Modified average mean square error |
|---|---|---|---|
| test201md.img | 2.3161 | 0.0649 | 0.0999 |
| test202md.img | 2.2135 | 0.0775 | 0.0456 |
| test203md.img | 2.0339 | 0.0588 | 0.0011 |
| test204md.img | 1.9885 | 0.0493 | 0.0001 |
| test221md.img | 2.4445 | 0.0512 | 0.0598 |
| test222md.img | 2.4440 | 0.0681 | 0.0595 |
| test223md.img | 2.2288 | 0.0550 | 0.0008 |
| test224md.img | 2.2161 | 0.0499 | 0.0003 |
| test241md.img | 2.6802 | 0.0403 | 0.0785 |
| test242md.img | 2.6783 | 0.0542 | 0.0774 |
| test243md.img | 2.5557 | 0.0535 | 0.0242 |
| test244md.img | 2.5318 | 0.0491 | 0.0174 |
| test261md.img | 2.9331 | 0.0337 | 0.1109 |
| test262md.img | 2.9033 | 0.0448 | 0.0920 |
| test263md.img | 2.8769 | 0.0481 | 0.0767 |
| test264md.img | 2.8401 | 0.0452 | 0.0576 |
| test281md.img | 3.1536 | 0.0304 | 0.1250 |
| test282md.img | 3.1113 | 0.0400 | 0.0969 |
| test283md.img | 3.1251 | 0.0413 | 0.1057 |
| test284md.img | 3.1089 | 0.0411 | 0.0954 |
| test301md.img | 3.3195 | 0.0287 | 0.1021 |
| test302md.img | 3.2743 | 0.0362 | 0.0752 |
| test303md.img | 3.2945 | 0.0359 | 0.0867 |
| test304md.img | 3.2991 | 0.0369 | 0.0895 |

*Files are mid-point displacement realizations with fractal dimensions 2.0, 2.2, 2.4, 2.6, 2.8, and 3.0.*

**Table 2. Mean, variance, and mamse of 250 × 250 fractal dimension arrays resulting from PE estimation on ensemble average PSD constructs.**

| File | Fractal dimension estimate | Variance | Modified average mean square error |
|---|---|---|---|
| n2psd201.img | 1.9760 | 0.0479 | 0.0006 |
| n2psd202.img | 1.9529 | 0.0272 | 0.0022 |
| n2psd203.img | 2.0356 | 0.0275 | 0.0013 |
| n2psd204.img | 2.0107 | 0.0498 | 0.0001 |
| n2psd221.img | 2.0853 | 0.0423 | 0.1147 |
| n2psd222.img | 2.0377 | 0.0240 | 0.0263 |
| n2psd223.img | 2.1528 | 0.0252 | 0.0022 |
| n2psd224.img | 2.1479 | 0.0430 | 0.0027 |
| n2psd241.img | 2.3306 | 0.0393 | 0.0048 |
| n2psd242.img | 2.2766 | 0.0239 | 0.0152 |
| n2psd243.img | 2.3969 | 0.0249 | 0.0000 |
| n2psd244.img | 2.4086 | 0.0385 | 0.0001 |
| n2psd261.img | 2.6247 | 0.0361 | 0.0006 |
| n2psd262.img | 2.5894 | 0.0242 | 0.0001 |
| n2psd263.img | 2.6907 | 0.0252 | 0.0082 |
| n2psd264.img | 2.7121 | 0.0358 | 0.0126 |
| n2psd281.img | 2.9198 | 0.0343 | 0.0144 |
| n2psd282.img | 2.9100 | 0.0252 | 0.0121 |
| n2psd283.img | 2.9794 | 0.0260 | 0.0322 |
| n2psd284.img | 3.0064 | 0.0344 | 0.0426 |
| n2psd301.img | 3.2008 | 0.0348 | 0.0403 |
| n2psd302.img | 3.2130 | 0.0283 | 0.0454 |
| n2psd303.img | 3.2408 | 0.0284 | 0.0580 |
| n2psd304.img | 3.2034 | 0.0323 | 0.0414 |

*Files are power spectral density ensemble average realizations with fractal dimensions 2.0, 2.2, 2.4, 2.6, 2.8, and 3.0.*

**Table 3. Mean, variance, and mamse of 250 × 250 fractal dimension array resulting from PE estimation on single realization PSD constructs.**

| File | Fractal dimension estimate | Variance | Modified average mean square error |
|---|---|---|---|
| sr2psd201.img | 2.0740 | 0.0562 | 0.0055 |
| sr2psd202.img | 1.9762 | 0.0322 | 0.0006 |
| sr2psd203.img | 2.1283 | 0.0594 | 0.0165 |
| sr2psd204.img | 2.0411 | 0.0280 | 0.0017 |
| sr2psd221.img | 2.1370 | 0.0312 | 0.0039 |
| sr2psd222.img | 2.2210 | 0.0535 | 0.0004 |
| sr2psd223.img | 2.2749 | 0.0526 | 0.0056 |
| sr2psd224.img | 2.2147 | 0.0277 | 0.0002 |
| sr2psd241.img | 2.3974 | 0.0308 | 0.0000 |
| sr2psd242.img | 2.4442 | 0.0438 | 0.0019 |
| sr2psd243.img | 2.4928 | 0.0434 | 0.0086 |
| sr2psd244.img | 2.4785 | 0.0291 | 0.0062 |
| sr2psd261.img | 2.6982 | 0.0305 | 0.0096 |
| sr2psd262.img | 2.7015 | 0.0376 | 0.0103 |
| sr2psd263.img | 2.7484 | 0.0386 | 0.0220 |
| sr2psd264.img | 2.7643 | 0.0301 | 0.0269 |
| sr2psd281.img | 2.9880 | 0.0311 | 0.0353 |
| sr2psd282.img | 2.9646 | 0.0339 | 0.0271 |
| sr2psd283.img | 3.0049 | 0.0361 | 0.0420 |
| sr2psd284.img | 3.0417 | 0.0322 | 0.0584 |
| sr2psd301.img | 3.2126 | 0.0312 | 0.0452 |
| sr2psd302.img | 3.2138 | 0.0331 | 0.0457 |
| sr2psd303.img | 3.2520 | 0.0361 | 0.0635 |
| sr2psd304.img | 3.2780 | 0.0338 | 0.0773 |

*Files are power spectral density single realizations with fractal dimensions 2.0, 2.2, 2.4, 2.6, 2.8, and 3.0.*

The trend in the increase of the mamse in both the single realizations and ensemble averages shows the difficulties in estimation of the higher dimensions using the rectangular window; however, the results at lower dimensions are very encouraging. The low variance indicates the uniformity of the globally generated fractal surfaces.

Figure 1 plots the various estimates obtained against fractal dimension. Figures 2 to 5 are representative surface plots and DFTs of the single-realization PSD and MPD surfaces produced by Gouraud shading with an overhead light source. A brief remark is in order about the DFT figures. They were created by taking a $32 \times 32$ section of the original $256 \times 256$ DFT (single realization) and displaying the absolute value of the spatial frequency coefficients from $(k,l) = (1,1)$ to $(k,l) = (32,32)$; the axes are reversed since the sample section was taken from the DFT region $(k,l) = (224,224)$ to $(k,l) = (255,255)$, which is analogous by symmetry.

Closer inspection of the MPD DFTs suggests that extra power resides along the spatial frequency axes, thus affecting the PE estimation algorithm, and, in fact, the reliability of the MPD method has been questioned before with regard to synthesizing fractal Brownian motion for any persistence parameter $H$ deviating from 1/2 [27]. The slight increase in the power residing along the spatial-frequency axis of the PSD DFTs can be accounted for by the inherent periodicity of the construct; therefore, $N/4 \times N/4$ samples as used in Moghaddam's work is probably preferred and may have led to a more accurate fractal sample. Figures 6 to 9 are representative of the 3-D surfaces produced by the different synthesis algorithms and show the rougher texturing of the MPD method for identical fractal dimensions. The original surfaces were constructed using floating-point representation; however, they were byte-scaled for 3-D plotting—thus the $z$-axis range of 0 to 255 in figures 6 to 9.

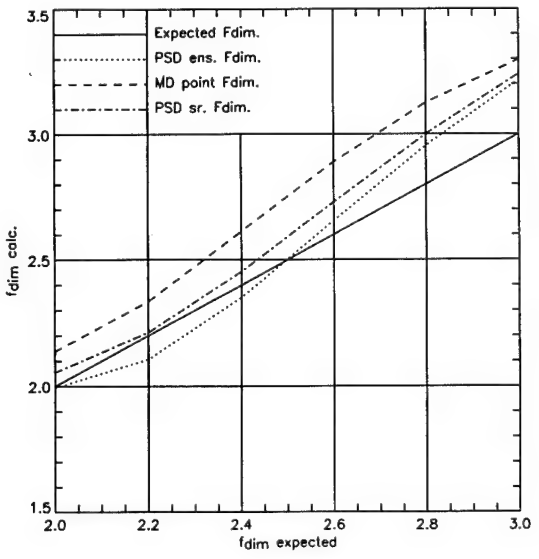


**Figure 1. Plot of global mean for each 512 × 512 block processed with PE estimation compared to global fractal dimension used in original synthesis of 512 × 512 constructs.**

**Figure 2. Synthetic fractal surfaces and corresponding DFTs created by single realization PSD and MPD methods with fractal dimension 2.0.**

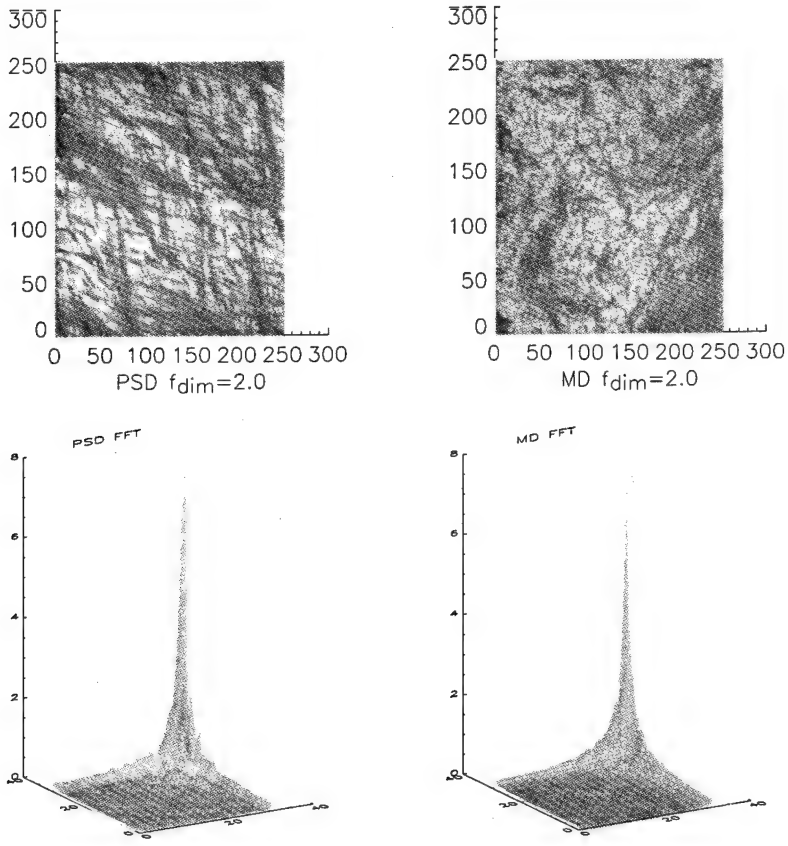


**Figure 3. Synthetic fractal surfaces and corresponding DFTs created by single realization PSD and MPD methods with fractal dimension 2.2.**

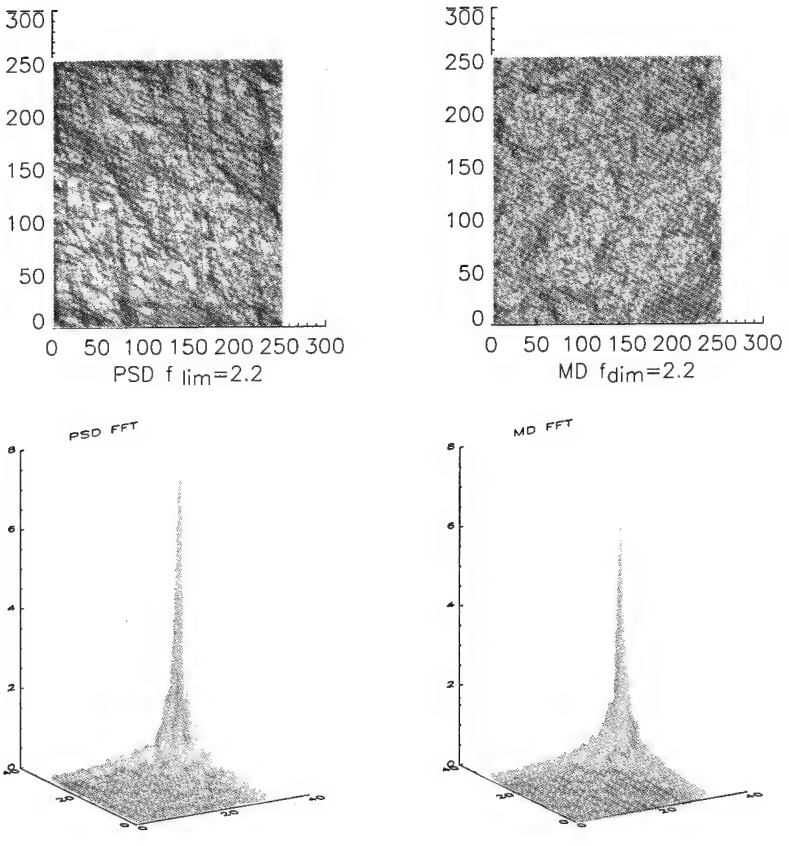

**Figure 4. Synthetic fractal surfaces and corresponding DFTs created by single realization PSD and MPD methods with fractal dimension 2.4.**

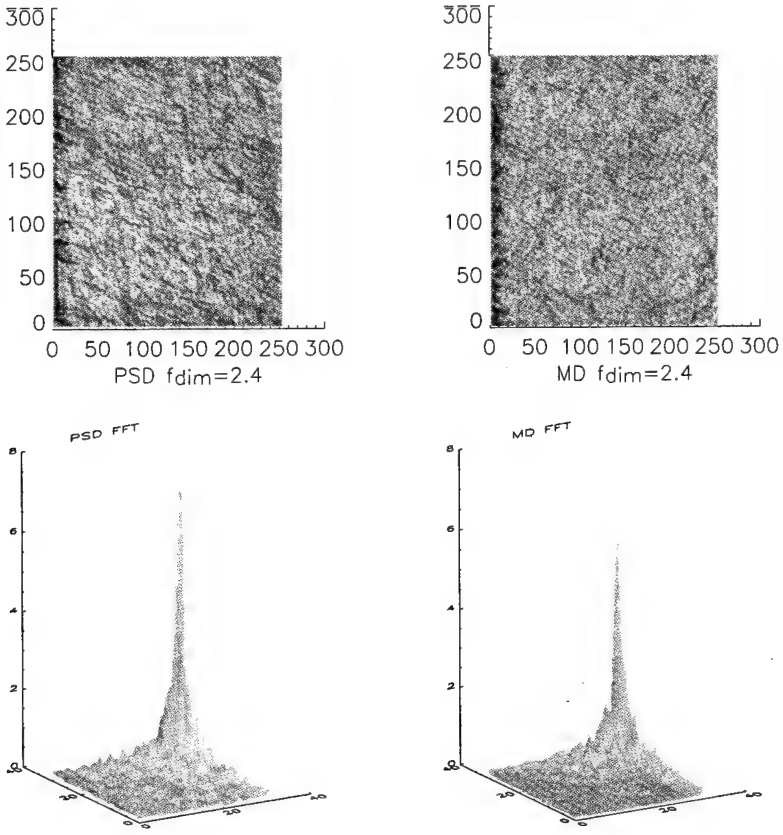


**Figure 5. Synthetic fractal surfaces and corresponding DFTs created by single realization PSD and MPD methods with fractal dimension 2.6.**

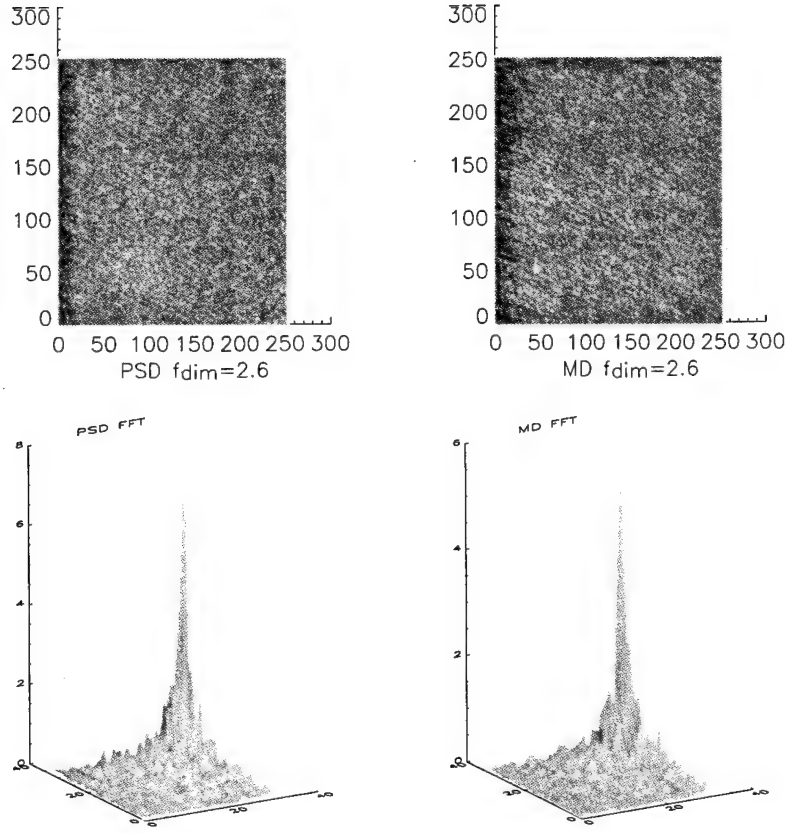

**Figure 6. Typical fractal surfaces synthesized by ensemble average PSD and MPD algorithms using a fractal dimension of 2.0.**

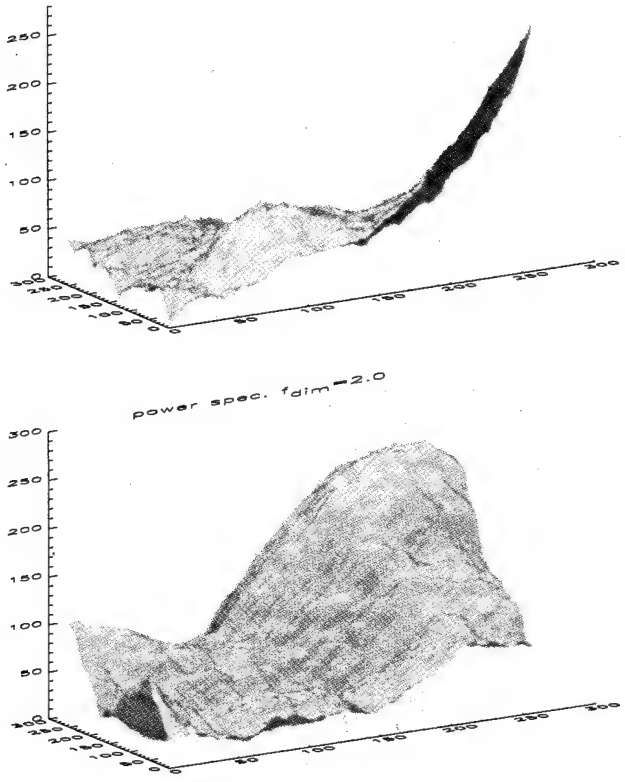


**Figure 7. Typical fractal surfaces synthesized by ensemble average PSD and MPD algorithms using a fractal dimension of 2.2.**

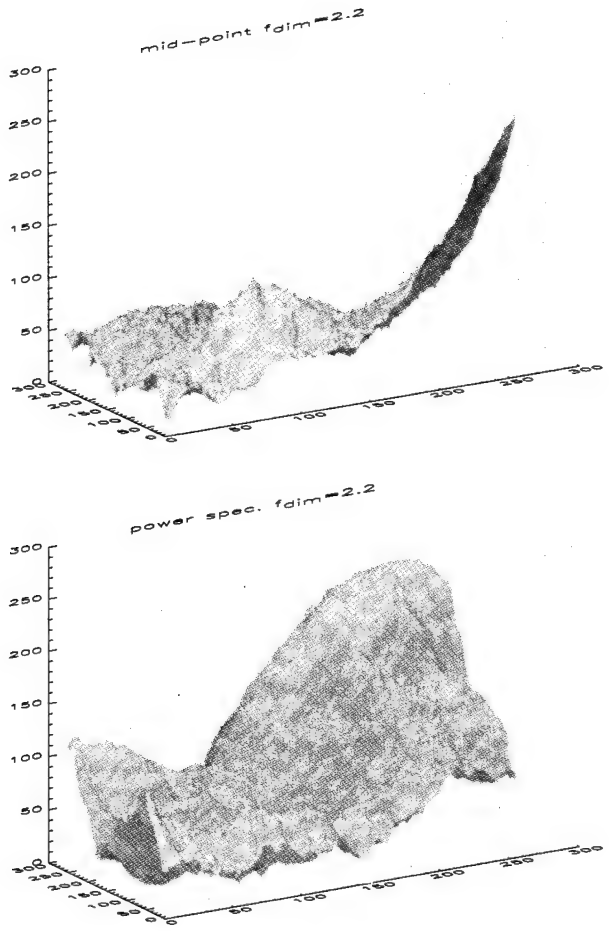

**Figure 8. Typical fractal surfaces synthesized by ensemble average PSD and MPD algorithms using a fractal dimension of 2.4.**

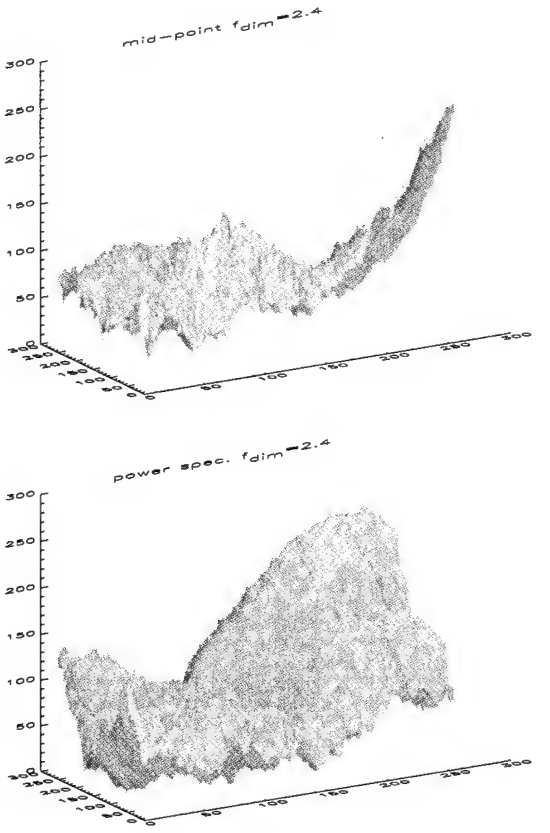


**Figure 9. Typical fractal surfaces synthesized by ensemble average PSD and MPD algorithms using a fractal dimension of 2.6.**

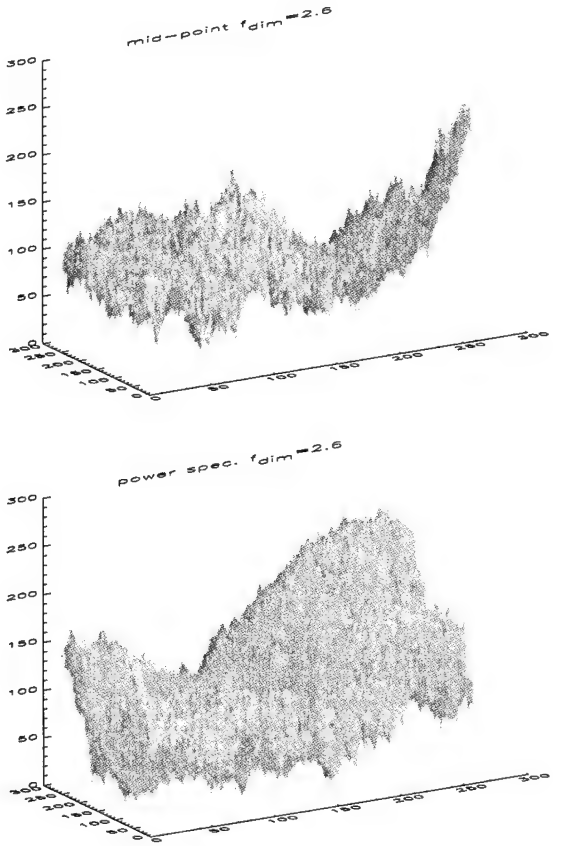

Table 4 shows the average values for the estimates in tables 1 to 3, and these average values for the fractal dimension are plotted in figure 1. The key in figure 1 indicates the three classes of images produced with "Expected Fdim," indicating a perfect estimate based on the fractal dimension used for synthesis, "PSD ens. Fdim," indicating the results of estimating the PSD ensemble average surfaces, "PSD sr. Fdim," indicating the results of estimating the PSD single realization surfaces and, last, "MD point Fdim," containing the results of estimation applied to the MPD synthesized surfaces. These results show quite clearly the tracking of the fractal dimension by the simple estimator over the desired range with an increasing deviation from the true fractal dimension after a 2.5 fractal dimension. Results similar to this were achieved with other seed values used in the random number generator for producing PSD surfaces as well.

The algorithm was developed using the PV-Wave command language and is currently not optimized for speed. The execution time for the algorithm has not been determined. The unoptimized PV-Wave version executes an estimation in 260 s, including the system overhead; this time is similar to Moghaddam's [29] optimized C version.

**Table 4. Global mean, variance, and mamse for each 512 × 512 block synthesized by three techniques and processed with PE estimator. (Expected fractal dimension is simply value used in original constructs.)**

| Fractal surface type | Expected fractal dimension | Calculated fractal dimension | Variance | Modified average mean square error |
|---|---|---|---|---|
| MPD method | | | | |
| | 2.0 | 2.1380 | 0.0622 | 0.0190 |
| | 2.2 | 2.3333 | 0.0558 | 0.0178 |
| | 2.4 | 2.6115 | 0.0491 | 0.0447 |
| | 2.6 | 2.8884 | 0.0428 | 0.0831 |
| | 2.8 | 3.1247 | 0.0381 | 0.1055 |
| | 3.0 | 3.2968 | 0.0344 | 0.0881 |
| PSD method ensemble average | | | | |
| | 2.0 | 1.9938 | 0.0373 | 0.0011 |
| | 2.2 | 2.1059 | 0.0330 | 0.0111 |
| | 2.4 | 2.3518 | 0.0312 | 0.0050 |
| | 2.6 | 2.6542 | 0.0301 | 0.0054 |
| | 2.8 | 2.9539 | 0.0298 | 0.0253 |
| | 3.0 | 3.2145 | 0.0309 | 0.0463 |
| PSD method single realization | | | | |
| | 2.0 | 2.0549 | 0.0429 | 0.0047 |
| | 2.2 | 2.2119 | 0.0403 | 0.0025 |
| | 2.4 | 2.4532 | 0.0364 | 0.0042 |
| | 2.6 | 2.7281 | 0.0341 | 0.0172 |
| | 2.8 | 2.9998 | 0.0333 | 0.0407 |
| | 3.0 | 3.2391 | 0.0335 | 0.0579 |

*Values are the averages from tables 1 to 3 with the calculated fractal dimensions plotted on plot 1.*

# 4. Conclusions

The PE method remains a possible candidate for "real-time" processing of the fractal dimension with subsequent texture classification and segmentation. The relatively low variance and mamse demonstrate the algorithm's accuracy over the limited range of interest.

The effect of the rectangular window was apparent at the higher dimensions due to side-lobe leakage and therefore must be questioned for the segmentation of tree clutter [13] and probably other types of clutter that exhibit a high fractal dimension. To circumvent this problem, an adaptive estimation routine may be useful that uses the results of Bovik and Super [9], together with the simple algorithm given here.

The estimator results show no significant difference between estimating the ensemble average as opposed to the single realizations. This should be expected since the DFTs of an $8 \times 8$ local window derived from the ensemble average are indistinct from those DFTs taken from single realizations. The only differences I observed were in taking global estimates (unpublished finding) of the surfaces and the slight increase in the variance. This indicates the viability of the estimation technique to "real terrain" (single realization) and not just well-behaved laboratory models.

The presence of artifacts within a mid-point displacement rendering [5] probably contributes to the extra power distributed along the spatial-frequency axis (see fig.1, lower right corner), thus perturbing the estimation of the fractal dimension. A path to further resolving this issue is in generating fractals using the random additions refinement to the MPD method and performing the estimation [5].

Future work will involve the optimization of the PSD synthesis routine and PE estimation algorithm in C and should be included in the KHOROS image-processing software for future use. An optimized version of the PE algorithm could reduce the processing time by, at minimum, a factor of four. Accurate measurements of the optimized code will be performed, as well as the texture analysis and segmentation of synthetic composite surfaces, natural surfaces, and SAR images.

# Acknowledgements

I would like to thank Dr. Joseph Sattler for his support and discussions on the nature of fractals as well as Scott Hayes, Roberto Innocenti, and Dave Wong for their helpful tips on PV-Wave.

# References


1. B. B. Mandelbrot and J. W. Wallis, "Fractional Brownian Motions, Fractional Noises, and Applications," *SIAM Rev.*, **10** (1968), 422–437.

2. B. B. Mandelbrot, *Fractals: Form, Chance, and Dimension,* W. H. Freeman and Co., San Francisco (1977).

3. B. B. Mandelbrot, *The Fractal Geometry of Nature*, W. H. Freeman and Co., New York (1982).

4. M. Barnesley, *Fractals Everywhere*, Academic Press, San Diego (1988).

5. H. O. Pietgen and D. Saupe, *The Science of Fractal Images*, Springer-Verlag, New York (1988).

6. T. Vicsek, *Fractal Growth Phenomenon*, World Scientific Pub. Co., Teaneck, New Jersey (1989).

7. A. P. Pentland, "Fractal Based Description of Natural Scenes," *IEEE Trans. Pattern Analysis and Machine Intelligence*, **PAMI-6**, 6 (November 1984), 661–674.

8. A. P. Pentland, "Shading into Texture," *Artif. Intel.*, **29** (1986), 147–170.

9. B. A. Super and A. C. Bovik, "Optimally Localized Estimation of the Fractal Dimension, Curves and Surface in Computer Vision and Graphics," *SPIE,* **1251** (1990), 357–368.

10. S. Peleg, J. Naor, R. Hartley, and D. Avnir, "Multiple Resolution Texture Analysis and Classification," *IEEE Trans. Pattern Analysis and Machine Intelligence*, **PAMI-6**, 4 (July 1984), 512–523.

11. J. M. Keller, S. Chen, and R. M. Crownover, "Texture Description and Segmentation through Fractal Geometry," in *Computer Vision, Graphics, and Image Processing*, **45** (1989), 150–166.

12. N. Yokoya, K. Yamamoto, and N. Funakubo, "Fractal Based Analysis and Interpolation of 3D Natural Surface Shapes and Their Application to Terrain Modeling," in *Computer Vision, Graphics, and Image Processing,* **46** (1989), 284–302.

13. C. V. Stewart, B. Moghaddam, K. J. Hintz, and L. M. Novak, "Fractional Brownian Motion Models for Synthetic Aperture Radar Imagery Scene Segmentation," Submitted to *Proc. IEEE*, Applications of Fractals in Electrical Engineering (1992).

14. M. C. Stein, "Fractal Image Models and Object Detection, Visual Communications and Image Processing II," *SPIE,* **845** (1987), 293–301.

15. C. Chen, J. S. Daponte, and M. D. Fox, "Fractal Feature Analysis and Classification in Medical Imaging," *IEEE Trans. Med. Imaging*, **8**, 2 (June 1989), 133–142.

16. A. Fournier, D. Fussell, and L. Carpenter, "Computer Rendering of Stochastic Models," *Commun. ACM*, **25**, 6 (1982), 371–384.

17. H. Tamura, S. Mori, and T. Tamawaki, "Textural Features Corresponding to Visual Perception," *IEEE Trans. Syst., Man, Cybern.*, **SMC-8** (June 1978), 460–473.

18. J. J. Freeman, *Principles of Noise*, John Wiley and Sons, Inc., New York (1958).

19. F. Rief, *Statistical and Thermal Physics*, McGraw Hill Book Co., New York (1965).

20. F. N. H. Robinson, *Noise and Fluctuations,* Clarendon Press, Oxford (1974).

21. P. Flandrin, "On the Spectrum of Fractional Brownian Motion," *IEEE Trans. Inf. Theory*, **35** (January 1989), 197–199.

22. M. S. Keshner, "1/f Noise," *Proc. IEEE*, **70** (March 1982), 212–218.

23. G. W. Wornell, "A Karhunen-Loeve-like Expansion for 1/f Processes via Wavelets," *IEEE Trans. Inf. Theory*, **36**, 4 (July 1990).

24. H. E. Schepers, J.H.G.M. Van Beek, and J. B. Bassingthwaighte, "Four Methods to Estimate the Fractal Dimension from Self-Affine Signals," *IEEE Engineering in Medicine and Biology* (June 1992), 57–71.

25. J. B. Bassingthwaighte and R. P. Beyer, "Fractal Correlation in Heterogenous Systems," *Physica D,* **53** (1991), 71–84.

26. C. Fortin, S. Hoefer, R. Kumaresan, and W. Ohley, "Fractal Dimension in the Analysis of Medical Images," *IEEE Engineering in Medicine and Biology* (June 1992), 65–71.

27. R. F. Voss, "Random Fractal Forgeries," *Fundamental Algorithms for Computer Graphics*, R. A Earnshaw, ed., **F17** Springer-Verlag, Berlin Germany (1985), 805–835.

28. K. J. Hintz, C. V. Stewart, and B. Moghaddam, "Characterization and Segmentation of Maritime IR Images Using Fractal Dimension," *SPIE*, Optical Engineering, submitted 1993.

29. B. Moghaddam, "Local Fractal Dimension Operators and Relaxation Techniques for Image Segmentation," MS Thesis, George Mason University, Fairfax VA (January 1992).

30. A. K. Jain, "Fundamentals of Digital Image Processing," Prentice Hall, Englewood Cliffs, New Jersey (1989).

31. R. F. Voss, *Random Fractals: Characterization and Measurement, Scaling Phenomena in Disordered Systems*, R. Pynn and A. Skjeltorp, eds., Plenum Press, New York (1986).

# Distribution

Admnstr
Defns Techl Info Ctr
Attn DTIC-DDA (2 copies)
Cameron Sta Bldg 5
Alexandria VA 22304-6145

Univ of MD Ctr for Automtn Rsrch
Attn R Chellappa
AVW Bldg Rm 2365
College Park MD 20742-2375

Univ of MD Dept of Elec Eng
Attn T Fuja
AV Williams RM 2161
College Park MD 20742

Univ of MD Dept of Elec Eng
Attn R Liu
AV Williams RM 2157
College Park MD 20742

Univ of MD Dept of Math
Attn J Benedetto
College Park MD 20742-4015

US Army Rsrch Lab
Attn AMSRL-D J W Lyons
Attn AMSRL-OP-SD-TA Mail & Records Mgmt
Attn AMSRL-OP-SD-TL Tech Library (3 copies)
Attn AMSRL-OP-SD-TP Tech Pub
Attn AMSRL-SS J Sattler
Attn AMSRL-SS J W Miller
Attn AMSRL-SS V DeMonte
Attn AMSRL-SS-SG H Khatri
Attn AMSRL-SS-SG P Alexander
Attn AMSRL-SS-SM J Eicke
Attn AMSRL-SS-SM R Kapoor
Attn AMSRL-SS-SM N Srour
Attn AMSRL-SS-SD H Dropkin
Attn AMSRL-SS-SH G Sztankay
Attn AMSRL-SS-SA M Wellman (6 copies)